Structure Formation in the Melt-Quenched Al−12.2Si−0.2Fe Alloys

O. V. Gusakova[a], *, V. G. Shepelevich[b], D. V. Alexandrov[c], **, and I. O. Starodumov[c]

[a]*International Sakharov Environmental Institute of Belarusian State University, Minsk, Belarus*
[b]*Belarusian State University, Minsk, Belarus*
[c]*Ural Federal University Named after the First President of Russia B.N. Yeltsin, Yekaterinburg, 620002 Russia*
*e-mail: ol.gusakova@gmail.com
**e-mail: dmitri.alexandrov@urfu.ru

Abstract—The microstructure, the phase composition, the component distribution, and the grain structure of the commercial eutectic Al−12.2 Si−0.2 Fe (at %) silumins formed at cooling rates of 10^2 and 10^5 K/s are studied. Three phases are detected in the alloy after solidification at both cooling rates: α-aluminum, silicon, and an iron-containing phase. The bulk samples have a heterogeneous dendritic structure with large dendrites of an aluminum-based solid solution, and a eutectic lamellar mixture of aluminum and silicon filling the interdendritic space. The melt-quenched foils are characterized by a homogeneous microstructure over the thickness; however, they have a layered structure. The rapidly solidified foils also have a homogeneous granular structure through the thickness and no pronounced texture. The mechanisms of solidification and microstructure formation are proposed for both the bulk samples and the melt-quenched foils.

INTRODUCTION

Silumins are the most widely used aluminum alloys, because they have unique technical characteristics, such as a low density, high mechanical properties, and a low linear thermal expansion coefficient [1, 2]. The focus is on improving their service and cast properties by reducing the silicon particle size. Increasing the solidification rate is one of the technologies that enable one to modify the structure and, thus, to increase the strength and ductility of Al−Si alloys.

Melt quenching is the most technological and resource-efficient technique for achieving high solidification rates. This technique is used to produce materials in the form of a foil as a result of solidification of a thin layer of a melt after it spreads over the surface of a rotating mold at a cooling rate of 10^5-10^7 K/s. An increase in the cooling rate of a melt is known to refine structural constituents [3]. For example, the size of silicon inclusions in silumin can be reduced by an order of magnitude in comparison with quasi-equilibrium solidification [4]. High-rate solidification increases the solubility above the equilibrium one [5]. The solubility of silicon in aluminum in Al−Si alloys was shown to be much higher than the equilibrium one [6, 7].

Alloys with eutectic or near-eutectic compositions are the most common in production. On the other hand, the laws of structure formation in eutectic alloys synthesized at high solidification rates are poorly investigated. Most works devoted to the solidification of eutectic alloys are theoretical and include the results of simulation [8], whereas the number of experimental studies is very small. Therefore, there is no generally accepted theoretically grounded and experimentally confirmed understanding about the structure-forming mechanisms in the eutectic alloys produced at high solidification rates. In particular, they include the theories of high-speed dendrite growth [9−11].

Most works on the microstructure of silumins concentrate on analysis of the size of silicon inclusions. The data on the granular structure of the aluminum phase are very scarce. Moreover, the considerations [12] about the α-Al grain sizes were not based on experimental data.

The aim of this work is to study the microstructure, the elemental composition, and the aluminum grain structure in eutectic silumin melt-quenched foils and bulk samples.

EXPERIMENTAL

The paper presents the investigation of commercial-purity silumin bulk samples and melt-quenched foils with the Al−12.2 Si−0.2 at % Fe eutectic composition (AK12och grade).
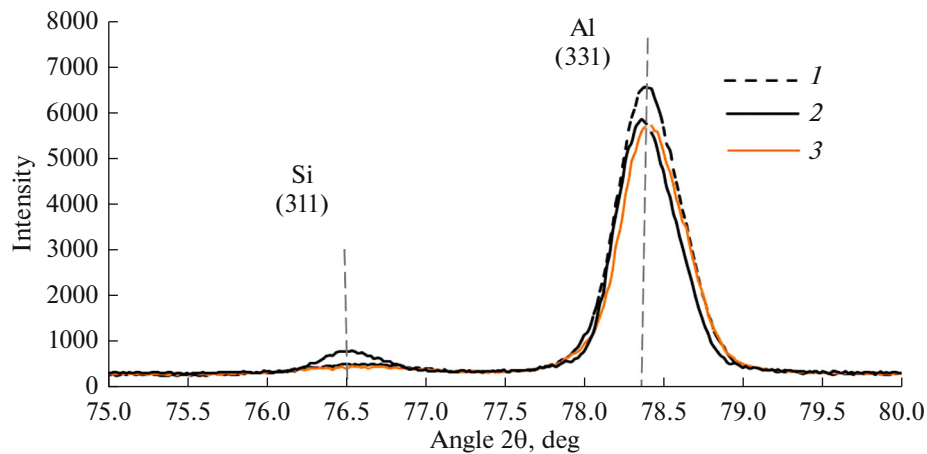
Fig. 1. X-ray diffraction patterns of (*1*) bulk sample and melt-quenched foil at (2) side adjacent to the mold and (*3*) freely-solidified side.

The bulk samples were produced by melt solidification in a graphite mold with a 3×6-mm^2 cross section. The melt cooling rate under these conditions was estimated to be 10^2 K/s. The foils were synthesized by rapid quenching from the melt. A melt drop was splashed onto the inner surface of a rotated hollow copper cylinder. The foils were 50−60 µm thick, up to 15 mm wide, and 8−10 cm long. The cooling rate in this technique was 10^5 K/s.

The elemental composition and distribution of components were determined using an Aztec Energy Advanced X-Max 80 energy dispersive microanalyzer.

The microstructure on both sides of the foil, as well as the cross-section of the foil, and in massive samples was examined using a LEO 1455VP scanning electron microscope equipped with a backscattered electron detector.

The grain structure in the rapidly solidified foils was analyzed by electron backscattered diffraction (EBSD) using an HKL EBSD Premium System Chennal 5 diffraction phase analyzer.

The samples were polished according to the Struers technique using a TegraPol 25 machine and cooling with water and special suspensions. At the last stage of polishing, a colloidal suspension containing silicon oxide with a particle size of 0.04 µm was employed to ensure delicate polishing without deforming the surface layer.

The phase composition of the foils was studied by X-ray diffraction (XRD) with a Rigaku Ultima IV diffractometer using copper $K\alpha_1$ and $K\alpha_2$ radiation at an average wavelength $\lambda = 1.54178$ Å.

RESULTS AND DISCUSSION

Comparative comprehensive studies of both rapidly solidified foils and bulk samples fabricated at a melt cooling rate of 10^2 K/s were carried out to identify structure-forming mechanisms in the alloy during rapid melt cooling more accurately.

Figure 1 shows the results of phase analysis (regions of XRD patterns) of (*1*) bulk sample and (2) rapidly-solidified AK12och alloy foil from the side adjacent to the mold and from the freely-solidified one. The silumins under study were found to solidify with the formation of the following three phases: an aluminum-based solid solution (α-Al), a silicon-based solid solution, and an Fe-containing Al−FeSi phase.

X-ray diffraction patterns show that the positions of aluminum and silicon peaks correspond to the diffraction angles of pure phases without dissolved impurities. However, numerous studies of a large number of materials show that melt quenching increases the solubility in contrast to the equilibrium one. However, since the aluminum and silicon ion radii are similar (0.053 nm for Al, 0.054 nm for Si), the formation of a silicon solid solution in aluminum does not change the aluminum lattice parameter significantly, which could be detected as a line shift in an XRD pattern. Since XRD analysis is not very informative in this situation, we performed additional studies using scanning electron microscopy and electron microprobe analysis to determine the silicon concentration in the aluminum phase.

Figures 2a and 2b show electron microscopy images of the bulk samples, which were taken at different magnifications. The atomic number of silicon is higher than the aluminum number; therefore, bright regions correspond to the silicon phase. The contrast between two phases is very low because of the very
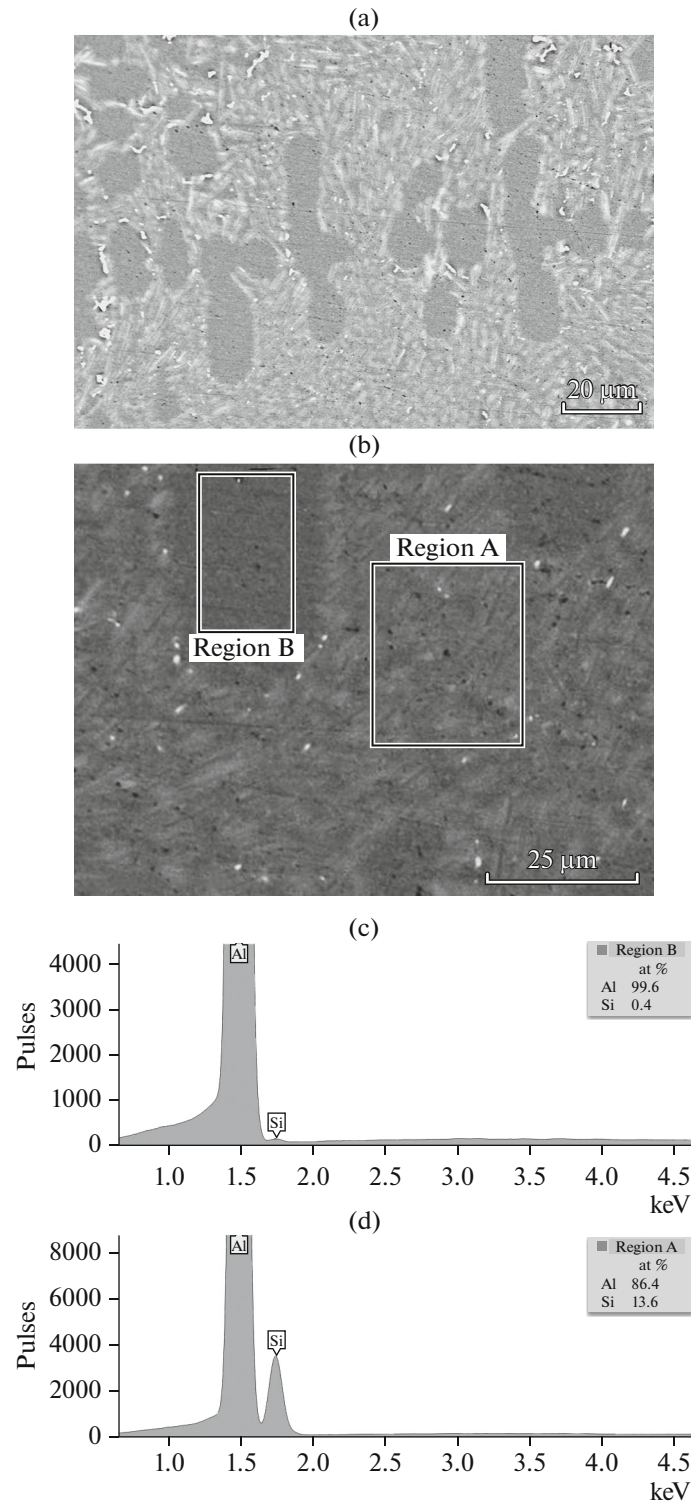
(a)

(b)

(c)

(d)

Fig. 2. (a), (b) Microstructure of the AK12och alloy synthesized at a cooling rate of 10^2 K/s and (c), (d) characteristic X-ray spectra of various regions in the alloy.

small difference in their atomic numbers (13 for Al, 14 for Si). However, despite weak contrast, the received electron microscopy images exhibit two types of regions with different microstructures and compositions. Figures 1a and 1b show the results of XRD microanalysis.
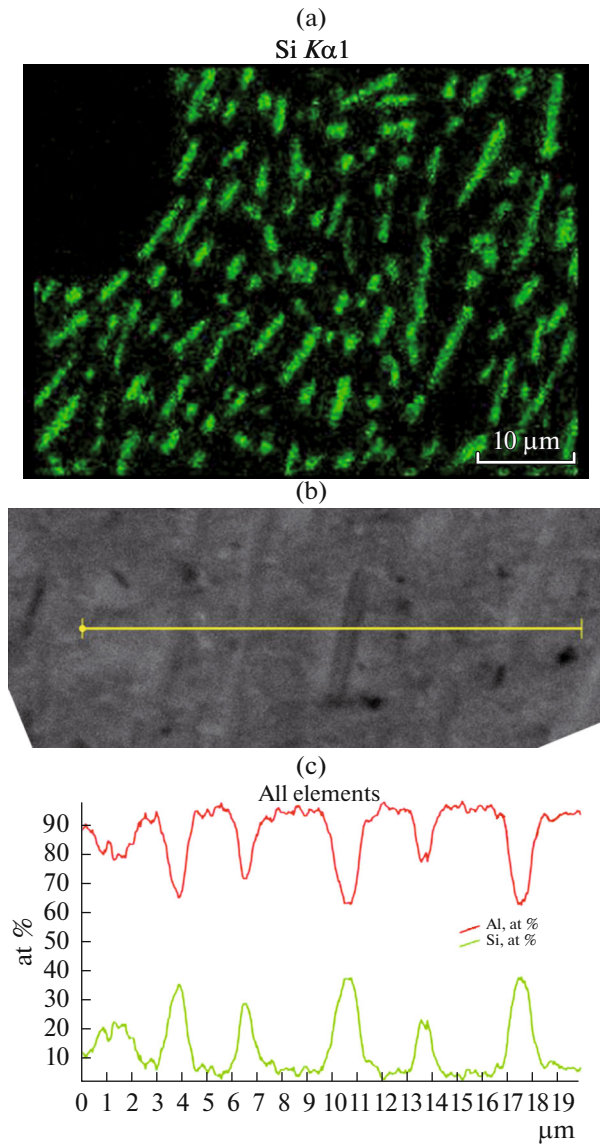
Fig. 3. (a) Microstructure and (b) distribution of elements in the AK12och alloy synthesized at a cooling rate of 10^2 K/s.

Regions A correspond to thin parallel lamellae of dark (Al) and bright (Si) phases. The length of these lamellae reaches 15−20 μm and their thickness is 2−3 μm. The silicon distribution maps and the component distribution survey along the scanning line, which are shown in the Fig. 3, confirm the lamellar structure in regions A.

No silicon or ternary compound inclusions are observed in regions B. As can be seen in Fig. 2a, the shape of these regions corresponds to dendritic branches. The size of these branches is about 10 μm. The composition examination (Figs. 2c, 2d) revealed 0.4 at % Si in regions B and 14.1 at % Si in regions A. Consequently, dendrites are a solid solution based on
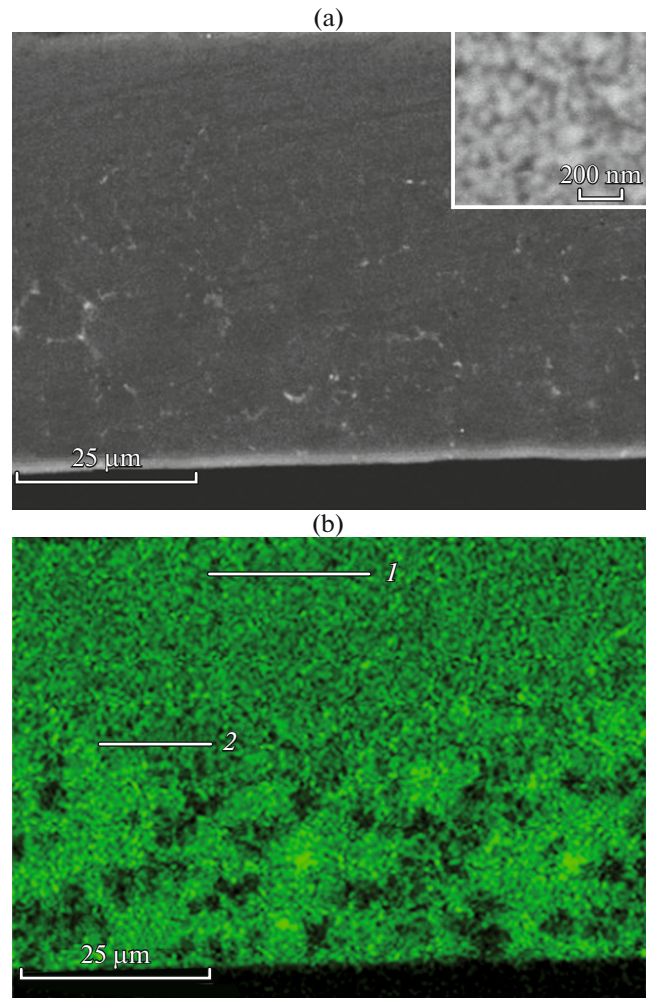

Fig. 4. (a) Microstructure and (b) distribution of elements in the AK12och alloy synthesized at a cooling rate of 10^5 K/s.

aluminum containing 0.4 at % silicon. This amount of dissolved silicon in the aluminum lattice insignificantly changes the aluminum lattice parameter and cannot be detected by XRD analysis, as was described above. The iron-containing phase is in the form of small globular inclusions mainly at the boundaries of aluminum-based dendrites and in the volume of regions A.

The structure described above is a typical dendritic structure of the AK12och alloy fabricated under quasi-equilibrium conditions [13]. This structure forms from the melt during solidification. Solidification starts from the growth of a primary aluminum solid solution in the form of dendrites. The interdendritic space solidifies as a lamellar eutectic, which contains aluminum and silicon phases. The Fe-containing phase forms at the dendritic boundaries at the final stage of solidification due to the forced displacement of iron
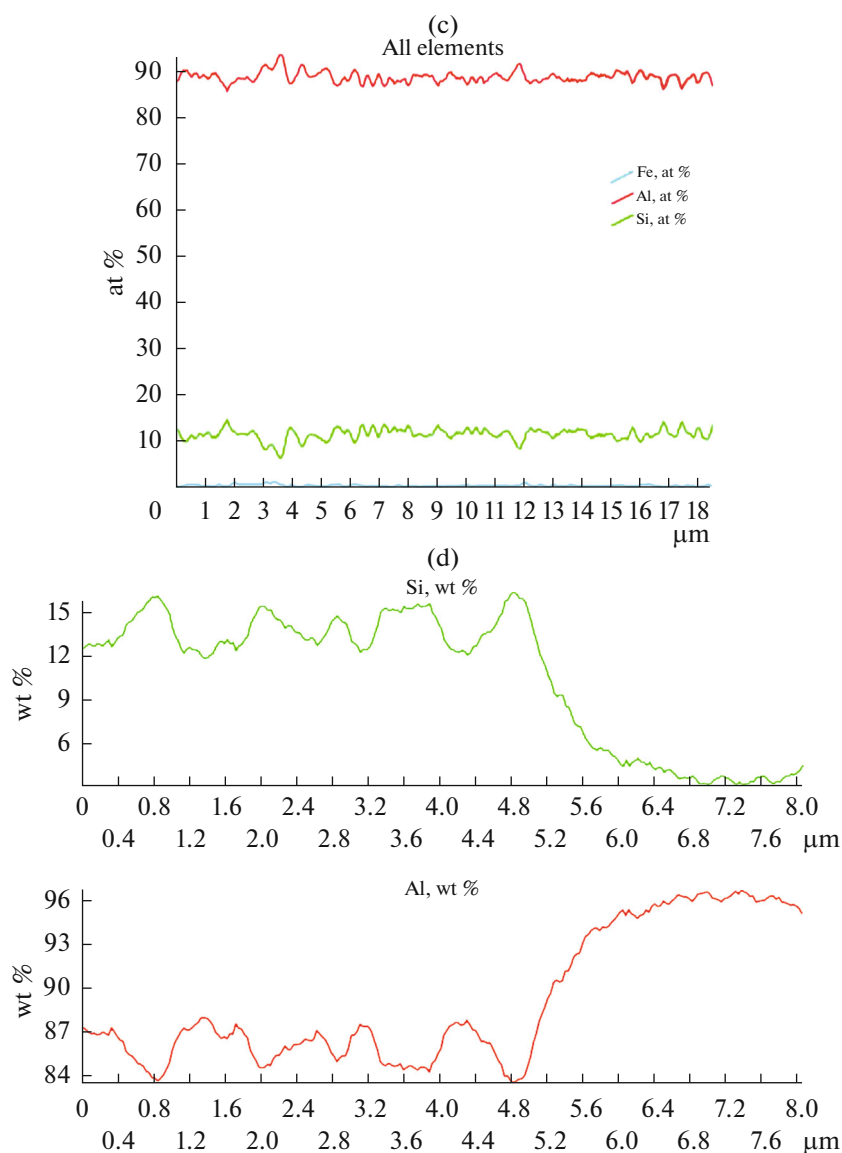
Fig. 4. (Contd.)

into the melt by the growing grains of the primary phase of the aluminum-based solid solution.

The microstructure of the rapidly solidified foils differs from that of the bulk samples in the uniformity of silicon distribution over the foil volume. However, the foils are layered across their thickness. The silicon distribution map (Fig. 4b) demonstrates inhomogeneity of silicon distribution on the freely-solidified side. Analysis of the elemental distribution along scanning lines (Figs. 4c, 4d) reveals a homogeneous Si distribution on the side adjacent to the mold and the presence of regions with different compositions on the opposite side. The silicon particle size on the side adjacent to the mold is 100−200 nm (see Fig. 3a). The distribution of elements along a scanning line demonstrates that

the size of silicon particles in the layer near the freely-solidified side does not exceed 500 nm (Fig. 4d). The Fe-containing phase precipitates along grain boundaries on the side adjacent to the mold.

These results were used to propose a model describing the formation of the experimentally observed layered microstructure in the rapidly-solidified AK12och alloy foils. This model takes into account the changes in solidification conditions across the thickness. As mentioned above, solidification takes place under highly nonequilibrium conditions in the foil production method. In this case, the rate of cooling and heat sink of the melt is maximal in the layer adjacent to the mold. This is the layer where a very high rate of displacement of the interface between
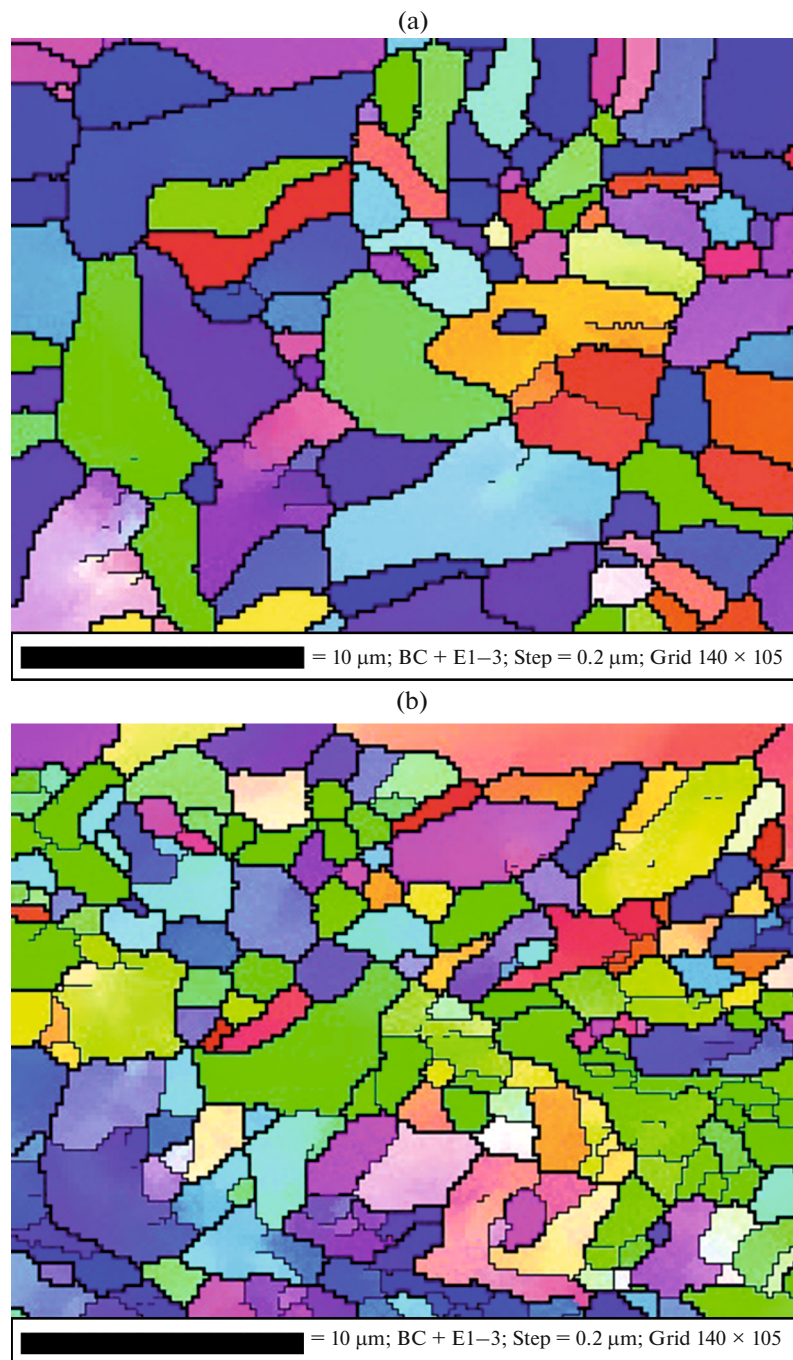
(a)

= 10 μm; BC + E1−3; Step = 0.2 μm; Grid 140 × 105

(b)

= 10 μm; BC + E1−3; Step = 0.2 μm; Grid 140 × 105

Fig. 5. (a, b) Grain structure and (c, d) direct pole figures of a rapidly quenching foil at (a, c) side adjacent to the mold and (b, d) freely-solidified side.

the liquid and solid phases, which becomes equal to or exceeds the diffusion rate of the impurities in the melt, can be achieved. Inseparable solidification conditions are fulfilled in this case.

The high solidification rate causes the growth of coarse grains of supersaturated Al-based solid solution. The observed microstructure of the foil layer adjacent to the mold results from the decomposition of the supersaturated solid solution. Nanoinclusions precipitate in the coarse Al grains in this layer. They uniformly fill the grain volume.

However, the released latent heat of solidification and the formation of a solidified bottom layer of the foil reduce the supercooling of the melt. This increases the temperature at the phase interface and, therefore, reduces the supercooling.
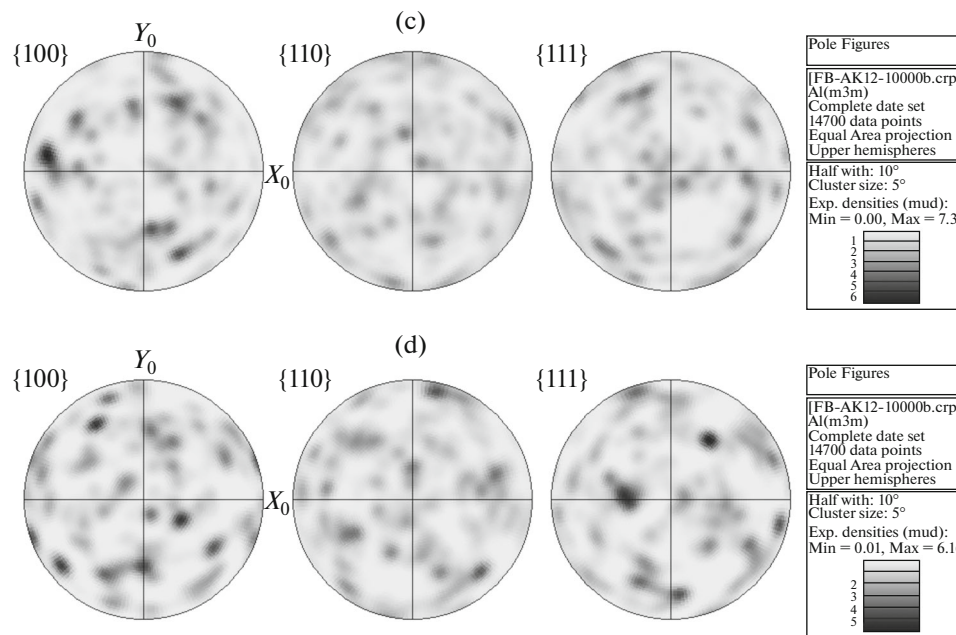
Fig. 5. (Contd.)

The final solidification stage proceeds at a reduced melt overcooling temperature and a temperature gradient, which initiates a solidification mechanism similar to the quasi-equilibrium solidification considered above. However, the cooling process remains significantly nonequilibrium in the rapidly solidified foil. Therefore, the sizes of silicon inclusions and primary α-Al dendrites are an order of magnitude smaller than those found in the samples formed at a melt cooling rate of 10^2 K/s.

The results of studying the grain structure in the foils are shown in Figs. 5a and 5b. Equiaxed grains with an average size of 4 μm form on both sides of the foil. The average grain size coincides with the average size of the regions bounded by an iron-containing compound (see Fig. 3a). Thus, the Al−FeSi phase is forced to grain boundaries in the melt during solidification. Analysis of pole figures showed no pronounced texture on both sides of the foil (Figs. 5c, 5d).

CONCLUSIONS

Melt quenching was found to modify the microstructure of eutectic silumins significantly. The melt-quenched foils have micron-sized grains and are characterized by a uniform distribution of grains and components over the foil thickness in comparison with bulk samples which are characterized by coarse regions with heterogeneous composition and structure. Layering of the microstructure was observed in the cross section of the foils. Nanoinclusions of silicon and Al−FeSi phases formed in the layer adjacent to the mold as a result of the decomposition of a supersaturated solid solution were detected. The solidification in the layer at the freely solidified side proceeds with the formation of dendrites of a silicon-rich (0.4 at %) α-Al solid solution and a eutectic mixture in the interdendritic space. The dendritic sizes do not exceed 3 μm.

REFERENCES

1. Y. Haizhi, "An overview of the development of Al−Si alloy based material for engine applications," J. Mater. Eng. Perform. **12**, 288−297 (2003).

2. R. Hernandez, C. Francisco, H. Ramirez, J. Martin, and R. Mackay, *Al−Si Alloys Automotive, Aeronautical, and Aerospace Applications* (Springer, 2017).

3. O. Gusakova, V. Shepelevich, and L. Scherbachenko, "Effect of melt cooling rate on microstructure of Sn−Bi and Sn−Pb eutectic alloys," Adv. Mater. Res. **856**, 236−240 (2014).

4. C. T. Rios, S. Santos, W. J. Botta, and C. Bolfarini "Microstructural characterization of as-quenched and heat treated Al−Si−Mg melt-spun ribbons," J. Metastable Nanocryst. Mater. **22**, 103−108 (2004).

5. O. Gusakova, V. Shepelevich, and L. Scherbachenko, "Aging of rapidly solidified eutectic Sn−Bi, Sn−Pb, Bi−Cd alloys," Perspekt. Mater. **5**, 25−32 (2016).

6. O. Uzun, T. Karaaslan, and M. Keskin, "Production and structure of rapidly solidified Al−Si," Turk. J. Phys. **25**, 455−466 (2001).

7. A. Bendijk, R. Delhez, L. Katgerman, Th. H. De Keijser, E. J. Mittemeijer, and N. M. Van Der Pers, "Characterization of Al−Si−alloys rapidly quenched from the melt," Mater. Sci. **15**, 2803−2810 (1980).

8. D. Herlach, P. Galenko, and D. Holland-Moritz, *Metastable Solids from Undercooled Melts*, (Elsevier, Amsterdam, 2007).

9. D. V. Alexandrov, D. A. Danilov, and P. K. Galenko, "Selection criterion of a stable dendrite growth in rapid solidification," Int. J. Heat Mass Transfer **101**, 789−799 (2016).

10. P. K. Galenko, D. A. Danilov, K. Reuther, D. V. Alexandrov, M. Rettenmayr, and D. M. Herlach, "Effect of convective flow on stable dendritic growth in rapid solidification of a binary alloy," J. Cryst. Growth. **457**, 349−355 (2017).

11. D. V. Alexandrov and P. K. Galenko, "Selected mode for rapidly growing needle-like dendrite controlled by heat and mass transport," Acta Mater. **137**, 64−70 (2017).

12. Q. Liu, M. Liu, C. Xu, W. Xiao, H. Yamagata, S. Xie, and C. Ma, "Effects of Sr, Ce and P on the microstructure and mechanical properties of rapidly solidified Al−7Si alloys," Mater. Charact. **140**, 290−298 (2018).

13. N. A. Belov, S. V. Savchenko, and A. V. Khvan, "Phase composition and structure of silumins," (MISiS, Moscow, 2007).

Translated by T. Gapontseva